THE JOURNAL OF BIOLOGICAL CHEMISTRY VOL. 284, NO. 2, pp. 1313–1323, January 9, 2009

Structural and Biochemical Characterization of the Wild Type PCSK9-EGF(AB) Complex and Natural Familial Hypercholesterolemia Mutants*[S]

Received for publication, November 3, 2008, and in revised form, November 7, 2008 Published, JBC Papers in Press, November 10, 2008, DOI 10.1074/jbc.M808363200

Matthew J. Bottomley[‡1], Agostino Cirillo[‡], Laura Orsatti[‡], Lionello Ruggeri[‡], Timothy S. Fisher[§], Joseph C. Santoro[§], Richard T. Cummings[§], Rose M. Cubbon[§], Paola Lo Surdo[‡], Alessandra Calzetta[‡], Alessia Noto[‡], Jennifer Baysarowich[§], Marco Mattu[‡], Fabio Talamo[‡], Raffaele De Francesco[‡2], Carl P. Sparrow[§], Ayesha Sitlani[§], and Andrea Carfí[‡3]

From the [‡]Department of Biochemistry, Istituto di Ricerca di Biologia Molecolare "P. Angeletti", Via Pontina Km 30.600, 00040 Pomezia (Rome), Italy and the [§]Division of Cardiovascular Diseases, Merck Research Laboratories, Rahway, New Jersey 07065

PCSK9 regulates low density lipoprotein receptor (LDLR) levels and consequently is a target for the prevention of atherosclerosis and coronary heart disease. Here we studied the interaction, of LDLR EGF(A/AB) repeats with PCSK9. We show that PCSK9 binds the EGF(AB) repeats in a pH-dependent manner. Although the PCSK9 C-terminal domain is not involved in LDLR binding, PCSK9 autocleavage is required. Moreover, we report the x-ray structure of the PCSK9ΔC-EGF(AB) complex at neutral pH. Compared with the low pH PCSK9-EGF(A) structure, the new structure revealed rearrangement of the EGF(A) His-306 side chain and disruption of the salt bridge with PCSK9 Asp-374, thus suggesting the basis for enhanced interaction at low pH. In addition, the structure of PCSK9ΔC bound to EGF(AB)^{H306Y}, a mutant associated with familial hypercholesterolemia (FH), reveals that the Tyr-306 side chain forms a hydrogen bond with PCSK9 Asp-374, thus mimicking His-306 in the low pH conformation. Consistently, Tyr-306 confers increased affinity for PCSK9. Importantly, we found that although the EGF(AB)^{H306Y}-PCSK9 interaction is pH-independent, LDLR^{H306Y} binds PCSK9 50-fold better at low pH, suggesting that factors other than His-306 contribute to the pH dependence of PCSK9-LDLR binding. Further, we determined the structures of EGF(AB) bound to PCSK9ΔC containing the FH-associated D374Y and D374H mutations, revealing additional interactions with EGF(A) mediated by Tyr-374/His-374 and providing a rationale for their disease phenotypes. Finally, we report the inhibitory properties of EGF repeats in a cellular assay measuring LDL uptake.

Proprotein convertase subtilisin-like/kexin type 9 (PCSK9)[4] has recently emerged as a major regulator of low density lipoprotein (LDL) cholesterol levels in plasma and consequently as an important determinant of cardiovascular health in humans. The link between cardiovascular disease and PCSK9 was initially made following the discovery that the *PCSK9* missense mutations, S127R and F216L (1), and later, D374Y (2), are associated with a form of autosomal dominant hypercholesterolemia, a risk factor for coronary heart disease. Subsequently, two *PCSK9* nonsense mutations (Y142*X* and C679*X*) (3) and several missense mutations (R46L, G106R, N157K, G236S, R237W, L253F, N354I and A443T) (4–6) have been found to be associated with hypocholesterolemia. Remarkable degrees of protection against coronary heart disease were observed in humans heterozygous for the mutations Y142*X* and C679*X* (88% reduced incidence) and by R46L (47% reduced incidence) (7). Consequently, PCSK9 represents a novel therapeutic target for the prevention of premature atherosclerosis and coronary heart disease, and an understanding of its mechanism of action is of significant medical interest.

PCSK9 is the ninth member of the mammalian proprotein convertase family of serine proteases. The translated proprotein includes an N-terminal signal sequence directing its secretion (residues 1–30), a prodomain (residues 31–152), a catalytic domain (residues 153–451), and a cysteine-rich C-terminal domain (residues 452–692) (8). PCSK9 undergoes autocleavage in the endoplasmic reticulum, and only the processed form is secreted (8, 9). The autocleavage event occurs between residues Gln-152 and Ser-153 and is dependent on a canonical triad of catalytic residues (Asp-186, His-226, and Ser-386). Unlike other members of the proprotein convertase family, following autocleavage the PCSK9 prodomain remains associated with the catalytic and C-terminal domains of the protein. The three-dimensional structure of this stable PCSK9 heterodimer as determined by x-ray crys-

* The costs of publication of this article were defrayed in part by the payment of page charges. This article must therefore be hereby marked "*advertisement*" in accordance with 18 U.S.C. Section 1734 solely to indicate this fact.

[S] The on-line version of this article (available at http://www.jbc.org) contains supplemental Figs. 1 and 2.

The atomic coordinates and structure factors (codes 2W2M, 2W2N, 2W2O, 2W2P, and 2W2Q) have been deposited in the Protein Data Bank, Research Collaboratory for Structural Bioinformatics, Rutgers University, New Brunswick, NJ (http://www.rcsb.org/).

[1] To whom correspondence may be addressed. Tel.: 39-06-91093-502; Fax: 39-06-91093-225; E-mail: matthew_bottomley@merck.com.

[2] Present address: Istituto Nazionale Genetica Molecolare, via Francesco Sforza 28, 20122 Milano, Italy.

[3] To whom correspondence may be addressed. Tel.: 39-06-91093-550; Fax: 39-06-91093-625; E-mail: andrea_carfi@merck.com.

[4] The abbreviations used are: PCSK9, proprotein convertase subtilisin-like/kexin type 9; LDL, low density lipoprotein; LDLR, LDL receptor; GOF, gain of function; TR-FRET, time-resolved fluorescence resonance energy transfer; WT, wild type; EGF, epidermal growth factor; FH, familial hypercholesterolemia; HEK, human embryonic kidney; MALDI, matrix-assisted laser desorption ionization; TOF, time-of-flight; MS, mass spectrometry; r.m.s.d., root mean square deviation.

tallography reveals a large noncovalent interface between the prodomain and the catalytic domain (10–12). A noteworthy feature of the interaction is that after autocleavage the C-terminal residues of the prodomain occupy the active site of the catalytic domain inhibiting further enzymatic activity by PCSK9.

PCSK9 is expressed predominantly in the liver, small intestine, and kidney (8). Recently, several independent groups have shown that processed PCSK9 binds to the LDL receptor (LDLR) and decreases total and cell surface LDLR levels by directing the receptor to the lysosomes for degradation (13). Although an intracellular mechanism preceding secretion is not formally excluded, the introduction of PCSK9 into the circulation of mice through parabiosis reduces hepatic LDLR levels (14), as does the injection into mice of recombinant PCSK9 (15, 16), suggesting that circulating PCSK9 can act by binding to LDLR on the cell surface. This *in vivo* study is further supported by *in vitro* experiments in which the addition of PCSK9 to cultured cell medium results in LDLR degradation (9, 14) and decreases LDL uptake (17). Prior to its degradation, the PCSK9-LDLR complex is internalized by endocytosis in a manner dependent on clathrin (18) and on the association of a cytosolic region of the LDLR with the ARH protein (14). A plausible mechanism of action leading to LDLR degradation rather than its vesicular recycling has been proposed following binding studies demonstrating that PCSK9 binds the LDLR ectodomain with ~100-fold higher affinity at the acidic pH of late endosomes/lysosomes compared with the neutral pH of the cell surface (10, 12, 17, 19). The enhanced affinity at acidic pH suggests that, differently from the LDLR-LDL complex, the LDLR-PCSK9 complex does not dissociate in the endosomes, thus preventing LDLR recycling and instead leading to shuttling of the complex to the lysosomes for degradation. Of note, the $PCSK9^{D374Y}$ mutant (a "gain-of-function" (GOF) mutant associated with hypercholesterolemia) was shown to bind the LDLR with 6–30-fold higher affinity than wild type (WT) PCSK9, supporting the notion that a tight interaction between PCSK9 and LDLR promotes degradation of the receptor.

Immunoprecipitation and Western blotting analyses were used by Hobbs and colleagues (19) to demonstrate that the epidermal growth factor-like repeat A (EGF(A)) of the LDLR is sufficient for PCSK9 binding. Recently, the x-ray crystal structure of the PCSK9-EGF(AB) complex, crystallized at pH 4.8, was also reported (20). Here we extend these data by characterizing the interaction, at both neutral and acidic pH, of the LDLR ectodomain and of the EGF(A) and EGF(AB) repeats of the LDLR with both full-length PCSK9 and a form of PCSK9 lacking the C-terminal domain (PCSK9ΔC). Moreover, we present the neutral pH x-ray crystal structure of WT PCSK9ΔC bound to EGF(AB) and the structures of mutant forms of these proteins associated with familial hypercholesterolemia (FH), including EGF(AB) bound to $PCSK9\Delta C^{D374Y}$ and $PCSK9\Delta C^{D374H}$, and of WT PCSK9ΔC bound to $EGF(AB)^{H306Y}$ (21–24). These structures reveal the molecular basis by which the mutations lead to FH. Further, comparisons of the previously reported low pH PCSK9-EGF(AB) complex structure with the structures reported here, and accompanying binding data, provide the molecular basis for the pH dependence of the PCSK9-EGF(A) interaction. Finally, we characterize the inhibitory properties of the isolated EGF repeats in a cellular LDL uptake assay demonstrating that *in vitro* these LDLR subfragments are sufficient to inhibit the LDLR-lowering activity mediated by PCSK9.

EXPERIMENTAL PROCEDURES

Preparation of Expression Plasmids

Full-length human PCSK9 with C-terminal V5 and His_6 epitope tags was cloned into the pcDNA3.1-F1-WT plasmid and expressed in stably transfected HEK293 cell lines as described previously (17). A modified form of the PCSK9 expression plasmid was also constructed to encode PCSK9 with the AviTag peptide sequence (GLNDIFEAQKIEWHE) between the V5 and His_6 tags, enabling site-specific biotinylation on the Lys (K) residue (underlined). The human LDLR ectodomain (residues 1–720) was cloned into the pDEST40 plasmid (Invitrogen) and the H306Y mutation was introduced.

DNA fragments encoding the proteins PCSK9ΔC (Gln-31—Ala-451) and ΔN-PCSK9ΔC (Ala-53—Ala-451) were subcloned from the pcDNA3.1-F1-WT plasmid into the pETM-10 expression plasmid (EMBL Heidelberg, Germany) which was subsequently modified to encode a C-terminal His_6 tag. The EGF(A) (Gly-293—Glu-332) and EGF(AB) (Gly-293—Lys-372) domains from human LDLR (numbering excludes N-terminal signal peptide) were cloned into the pETM-11 expression plasmid, which allows removal of the His_6 tag by digestion with tobacco etch virus protease (EMBL Heidelberg). All point mutations were introduced using the QuikChange site-directed mutagenesis kit (Stratagene).

Purification of Recombinant PCSK9, Biotinylated PCSK9, PCSK9ΔC, LDLR EGF Domain Proteins, and $LDLR^{H306Y}$ Ectodomain

Full-length PCSK9 and PCSK9-AviTag were expressed following stable transfection of HEK293 cells and purified as described previously (17). Purified PCSK9-AviTag was biotinylated *in vitro* with biotin ligase following the manufacturer's instructions (Avidity, Inc.). The PCSK9ΔC, ΔN-PCSK9ΔC, EGF(A), and EGF(AB) proteins were produced in *Escherichia coli* BL21 cells with induction of protein production by 0.4 mM isopropyl 1-thio-β-D-galactopyranoside and subsequent incubation with shaking at 18 °C overnight. After cell lysis, proteins were purified from the soluble fraction by nickel affinity chromatography. The EGF(A) and EGF(AB) proteins were then reduced by the addition of 0.1 M dithiothreitol and subjected to a 72-h oxido-shuffling refolding protocol by dialysis against 50 mM Tris-HCl, pH 8.3, 5% glycerol, 5 mM $CaCl_2$, 3 mM L-cysteine, and 0.3 mM L-cystine as described previously (25). The N-terminal His_6 tag was removed from the EGF(A/AB) proteins by overnight incubation at room temperature with a solubility-enhanced tobacco etch virus protease (26). All proteins were purified by size exclusion chromatography using a Superdex-75 (16/60 or 26/60) column equilibrated in 40 mM Tris-HCl, pH 7.5, 200 mM NaCl, 5% glycerol, 5 mM $CaCl_2$ for EGF proteins and in 40 mM Tris-HCl, pH 8.0, 200 mM NaCl, 5% glycerol, 0.1 mM $CaCl_2$, 0.05% *n*-octyl-β-glucoside for PCSK9ΔC and ΔN-PCSK9ΔC.

The LDLR^{H306Y} protein was produced in HEK293-EBNA cells following transient transfection. Cell supernatants were exchanged by ultrafiltration into buffer containing 50 mM sodium phosphate, pH 8.0, 300 mM NaCl, 1 mM $CaCl_2$, and the protein was purified by metal affinity chromatography (TALON resin, Clontech), followed by ion exchange chromatography (Resource Q, GE Healthcare) and size exclusion chromatography (Superdex 200, GE Healthcare) in 25 mM Hepes, pH 8.0, 150 mM NaCl, and 1 mM $CaCl_2$.

Surface Plasmon Resonance (SPR)

All SPR experiments were performed using Biacore instruments at 25 °C. Running buffers contained 150 mM NaCl, 1 mM $CaCl_2$, 0.005% (v/v) P-20 surfactant, and either 25 mM Hepes, pH 7.4, or 25 mM sodium acetate, pH 5.7. For studies of EGF(AB) binding to PCSK9, the purified full-length C-terminally biotinylated PCSK9 was noncovalently immobilized on a streptavidin-coated sensor surface (SA chip, GE Healthcare). For studies of PCSK9 or PCSK9ΔC binding to LDLR proteins, the purified full-length LDLR (WT or H306Y mutant) was covalently immobilized by amine coupling to a carboxymethylated dextran sensor surface (CM5 chip, GE Healthcare).

Binding constants were obtained from a series of injections at 50 μl/min of analyte (PCSK9, PCSK9ΔC, or EGF(AB)) at concentrations up to 2 μM. Following injections of PCSK9 or PCSK9ΔC, LDLR-coupled sensor chip surfaces were regenerated with a 5-s injection of 30 mM NaOH. Following injections of EGF(AB), the PCSK9-coupled sensor chip surface was regenerated with a 25-s injection of 5 mM EDTA followed by a 30-s injection of 6 mM $CaCl_2$. Data were analyzed using BIAevaluation software, with reference sensorgrams subtracted from experimental sensorgrams to yield curves representing specific binding. Steady-state analysis was used to plot equilibrium binding response (R_{eq}) against analyte concentration in order to obtain thermodynamic dissociation constants (K_D). For each series, simultaneous fitting of dissociation curves was used to obtain k_{off}, which was then used to obtain k_{on} ($K_D = k_{off}/k_{on}$) as described previously (17).

Time-resolved Fluorescence Resonance Energy Transfer (TR-FRET)

TR-FRET experiments were performed essentially as described previously (17) using 4 nM Eu^{3+}-labeled LDLR ectodomain and 10 nM Alexa Fluor 647-labeled PCSK9. Reactions were performed at 20 °C in 50 μl of buffer containing 10 mM Hepes, pH 7.4, 150 mM NaCl, 0.1 mM $CaCl_2$, and 0.05% (w/v) bovine serum albumin. Disruption of the PCSK9-LDLR interaction was assessed in titrations in which putative competitor proteins, typically in concentration ranges of 0.1 nM to 2.5 μM, were added to the reaction mixture with incubations for 16 h prior to fluorescence measurements. IC_{50} values were determined from triplicate experiments by fitting data to a sigmoidal dose-response curve using nonlinear regression (GraphPad Software Inc.). For proteins that did not give full titrations, data were fitted with the dose-response minimum defined by the signal obtained in the presence of 1 mM EDTA, which renders LDLR inactive.

LDL Uptake Assay

LDL uptake was measured in HEK293 cells stably expressing the pcDNA3.1 vector alone as described previously (17). The only experimental difference is that Alexa Fluor 546-labeled LDL, rather than LDL labeled with 3,3-dioctadecylindocarbocyanine (Dil), was used to follow cellular LDL uptake; labeling was performed as described previously (27). The inhibition of PCSK9 activity was assessed in titrations in which putative competitor proteins, in the nanomolar to micromolar concentration range, were added to the growth medium at the same time as PCSK9 followed by a 6.5-h incubation at 37 °C. The amount of competitor protein required for half-maximal inhibition of PCSK9 (IC_{50}) was determined by fitting data to a sigmoidal dose-response curve using nonlinear regression (GraphPad Software Inc.).

Epitope Excision and Mass Spectrometry

Immobilization of EGF(AB) on Sepharose Beads and Complex Formation with PCSK9^{D374Y}—CNBr-activated Sepharose beads (50 mg/ml) were resuspended in 1 mM HCl. A 100-μl volume of beads was packed into two 0.8-ml micro-columns and washed extensively with 1 mM HCl. The two columns were washed with 20 ml of 0.1 M $NaHCO_3$, 0.5 M NaCl, pH 8.3 (equilibration buffer), and the coupling reaction was performed for 2 h at 37 °C using either 50 μg of EGF(AB) in 200 μl of equilibration buffer or simply the equilibration buffer in the absence of EGF(AB) (control column). After coupling the columns were washed with 0.1 M Tris-HCl, pH 8.0, 0.5 M NaCl, then were incubated in the same buffer at 37 °C for 2 h to achieve complete deactivation of the Sepharose beads, and finally were washed with phosphate-buffered saline, pH 7.4. EGF(AB)-coupled beads and control beads were incubated with 0.1 μg/μl PCSK9^{D374Y} in 200 μl of phosphate-buffered saline for 2 h at 37 °C. The beads were then washed with 20 ml of phosphate-buffered saline.

Epitope Excision with Endoproteases—The complex-bound beads and the control beads were incubated with several endoproteases: chymotrypsin and AspN (1 μg/100 μl), trypsin (0.5 μg/100 μl), GluC (5 μg/100 μl), and aminopeptidase (100 μg/100 μl). Enzyme addition was repeated until the mass spectrum profile of the peptides bound to the EGF(AB)-coupled beads remained unchanged. The enzymes were added in the following order in four independent experiments: 1) chymotrypsin followed by trypsin, 2) GluC and aminopeptidase, 3) chymotrypsin followed by AspN, 4) trypsin followed by aminopeptidase.

MALDI-TOF MS Analysis—The peptides associated with the Sepharose beads were analyzed by MALDI-TOF MS. 1 μl of EGF(AB)-coupled beads was deposited on a MALDI target, and a saturated solution of sinapinic acid (3,5-dimethoxy-4-hydroxycinnamic acid; Aldrich) in 50% acetonitrile and 1% trifluoroacetic acid was added. The spectra of positive ions were recorded in linear mode on a MALDI-TOF mass spectrometer (Voyager-STR, Perseptive Biosystem, Inc., Framingham, MA) equipped with a delayed extraction device and a nitrogen laser (λ = 337 nm). Approximately 500 shots were averaged for each spectrum acquired. External calibration was performed with Glu1-FibrinopeptideB, ACTH-(1–17), ACTH-(18–39), and

ACTH-(7–38) using the monoprotonated ion of the monomers with average mass-to-charge (m/z) ratios. The difference between the calculated average mass and the experimental mass determination (0.05–0.1%) was consistent with the accuracy of MALDI-TOF mass spectrometry in linear mode.

ΔN-PCSK9ΔC-EGF(AB) Complex Crystallization and Structure Determination

Purified ΔN-PCSK9ΔC and EGF(AB) WT or mutant proteins were mixed in a 1:3 molar ratio, and the complex was separated from excess EGF(AB) by size exclusion chromatography on a Superdex-200 (26/60) column equilibrated in 40 mM Tris-HCl, pH 8.0, 200 mM NaCl, 20 μM $CaCl_2$, and 5% glycerol. The complex was concentrated to 4 mg/ml in a buffer containing 40 mM Tris-HCl, pH 8.0, 100 mM NaCl, 20 μM $CaCl_2$, and 5% glycerol and was crystallized by the vapor diffusion method. Crystals of WT ΔN-PCSK9ΔC with WT EGF(AB) were obtained using a reservoir containing 0.1 M Hepes, pH 7.5, 10% (v/v) 2-propanol, and 20% polyethylene glycol 4000. Crystals for all other complexes were obtained using a reservoir containing 0.1 M Hepes, pH 7.5, 10% polyethylene glycol 8000, and 8% ethylene glycol. Before data collection, crystals were transferred into stabilizing reservoir solutions containing increased precipitant concentration and 20% glycerol as cryoprotectant and were flash-frozen in liquid nitrogen.

X-ray diffraction data were collected at 100 K on the ID-23 beam line at the European Synchrotron Radiation Facility (ESRF, Grenoble, France). Diffraction data were processed with MOSFLM (28), and the CCP4 suite of programs (29) was used for further data processing and analysis. All crystals belong to the $P4_32_12$ space group and contain one ΔN-PCSK9ΔC-EGF(AB) complex per asymmetric unit and 65–70% solvent. The ΔN-PCSK9ΔC-EGF(AB) WT structure was determined by the molecular replacement method with PHASER (30) using the structure of PCSK9 (2QTW) with the C-terminal domain removed as a search model. After rigid body refinement, $2|F_o|-|F_c|$ electron density maps were calculated and used to build the LDLR EGF(A) domain. Model building was performed within Coot (31), and REFMAC (32) was used for structure refinement defining one TLS group per protein chain. The final models include residues Thr-60—Ser-447 of PCSK9 and Gly-293—Glu-332 of EGF(A). No electron density was observed for the EGF(B) domain, which is presumed to be disordered in the crystals. The amount of solvent-accessible surface area buried by protein complex formation was determined using the PISA software (33).

RESULTS

Processed PCSK9 Binds to the EGF(AB) Repeats of LDLR in a pH-dependent Manner—It has been reported that the EGF(A) domain of the LDLR receptor is sufficient to bind to PCSK9 (19, 20). To probe the affinities of the PCSK9-EGF(A) and PCSK9-EGF(AB) interactions and to compare them with the affinity of the PCSK9-LDLR complex, we used a TR-FRET assay. In this assay, EGF(A) and EGF(AB) competed efficiently with labeled LDLR for binding to labeled PCSK9, showing inhibition constants (IC_{50}) of 1255 ± 7 and 367 ± 94 nM, respectively, compared with an IC_{50} of 218 ± 41 nM when using unlabeled LDLR as a competitor (Fig. 1*A*). Thus, at neutral pH the EGF(AB) fragment bound to PCSK9 with an affinity similar to that of the full-length receptor.

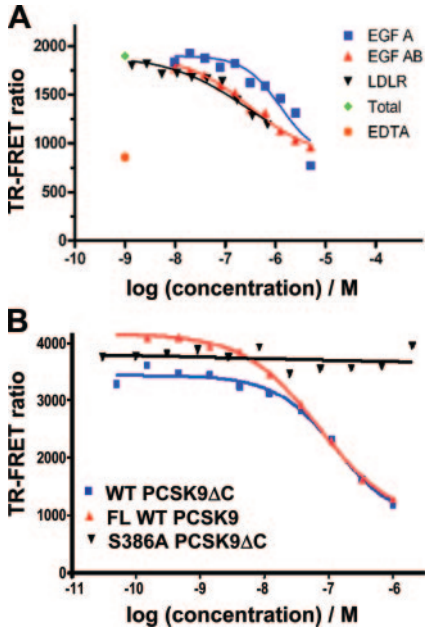

FIGURE 1. **TR-FRET analyses of the PCSK9-LDLR interaction and its inhibition.** *A*, in a TR-FRET assay at neutral pH, EGF(A) and EGF(AB) compete with the LDLR ectodomain for binding to PCSK9 with low/submicromolar IC_{50} values. *B*, in the TR-FRET assay, full-length WT PCSK9 and WT PCSK9ΔC are equipotent at disrupting the interaction of labeled WT PCSK9 with labeled LDLR, demonstrating that the C-terminal domain of PCSK9 is not required for binding. In contrast with WT PCSK9ΔC, an unprocessed form of PCSK9ΔC (S386A) was unable to disrupt the interaction.

Using SPR we showed previously that at neutral pH full-length WT PCSK9 binds to the LDLR ectodomain (residues 22–788) with a high nanomolar dissociation constant (K_D) and that this affinity is enhanced ~150-fold at acidic pH (17). Here we used SPR to examine the effect of pH on the interaction between PCSK9 and EGF(AB). Although covalently immobilized EGF(A) or EGF(AB) displayed specific binding to both PCSK9 and PCSK9ΔC, it was not possible to establish reliable surface regeneration conditions after successive analyte injections, and hence stepwise titrations in this format (EGF(A) or EGF(AB) proteins immobilized on sensor chip) were not feasible. Nevertheless, comparing equimolar (200 nM) protein injections at neutral or acidic pH, we consistently observed a greater response at acidic pH for binding of both PCSK9 and PCSK9ΔC to immobilized EGF(A) or EGF(AB) (supplemental Fig. 1*A*). Similarly, the $PCSK9^{D374Y}$ mutant also showed enhanced binding to immobilized EGF(A) or EGF(AB) at acidic pH (supplemental Fig. 1*B*). To confirm these observations and to obtain K_D values for the PCSK9-EGF(AB) interaction, we performed the reciprocal SPR analysis, in which a biotinylated form of PCSK9 was immobilized on a streptavidin-coated sensor chip. For this purpose, a PCSK9 protein with an additional C-terminal peptide sequence enabling site-specific *in vivo* biotinylation was prepared; the advantage was that this form of PCSK9 is immobilized on the sensor chip via the biotinylated C-terminal extension, with a reduced possibility of masking potential EGF(AB) binding sites. As observed previously for full-length LDLR at neutral pH, the EGF(AB) fragment bound to the

TABLE 1

Summary of binding data from surface plasmon resonance studies

"Ligand" refers to the immobilized protein, and "Analyte" refers to the protein injected in solution. §, in this assay format, k_{on} and k_{off} were not readily determined by fitting to the 1:1 Langmuir model, likely because of mass transfer limitation and incomplete dissociation of EGF(AB) from the surface. ND, not determined (the PCSK9ΔC protein was not sufficiently stable in solution at acidic pH to perform these measurements).

Ligand	Analyte	Neutral pH			Acidic pH		
		K_D	k_{off}	k_{on}	K_D	k_{off}	k_{on}
		nM	s^{-1}	$M^{-1}\cdot s^{-1}$	nM	s^{-1}	$M^{-1}\cdot s^{-1}$
PCSK9	EGF(AB)	340	§	§	140	§	§
LDLR	PCSK9ΔC	196	1.9×10^{-3}	9.7×10^{3}	ND	ND	ND
$LDLR^{H306Y}$	PCSK9	330	1.3×10^{-3}	3.8×10^{3}	7	0.6×10^{-3}	8.6×10^{5}

immobilized PCSK9 with a high nanomolar binding affinity (K_D = 340 nM; Table 1). Moreover, the affinity of the EGF(AB)-PCSK9 interaction was greater at acidic pH compared with neutral pH, exhibiting an ~3-fold enhancement in binding (K_D = 140 nM). Thus, in agreement with the TR-FRET assay results described above, the SPR data confirmed that the LDLR EGF(AB) fragment was sufficient for high affinity binding to PCSK9 and that the interaction was pH-dependent.

The PCSK9 C-terminal Domain Is Not Involved in LDLR Binding—A previous study had suggested that PCSK9 requires its C-terminal domain for LDLR binding (10). To evaluate the contribution of this region of PCSK9 for receptor binding we expressed in *E. coli* a truncated form of PCSK9 (PCSK9ΔC; residues 31–451) that lacks the entire C-terminal domain and tested this purified, autoprocessed protein in the TR-FRET assay. We found that the PCSK9ΔC protein was essentially as efficient as full-length PCSK9 at disrupting the PCSK9-LDLR interaction (Fig. 1*B*), exhibiting IC_{50} values of ~110 and ~80 nM, respectively. Further, SPR studies at neutral pH also revealed that PCSK9ΔC bound to LDLR with an affinity (K_D = 196 nM; Table 1) comparable with that exhibited by full-length PCSK9. Because of its poor solubility at low pH, the binding constants could not be determined for PCSK9ΔC at pH 5.7. Together these results demonstrate that at neutral pH the PCSK9 C-terminal domain (residues 452–692) is not involved in receptor binding.

PCSK9 Autocleavage Is Required for Effective Binding to LDLR—To assess whether PCSK9 autoprocessing is required for LDLR binding, we also expressed and purified an unprocessed form of PCSK9ΔC where the active site catalytic residue Ser-386 was mutated to alanine. The unprocessed S386A PCSK9ΔC protein was unable to disrupt the PCSK9-LDLR complex even when added in a 500-fold molar excess compared with processed PCSK9 (Fig. 1*B*). These results are consistent with a previous report stating that an uncleaved full-length catalytically inactive mutant PCSK9 was unable to bind LDLR *in vitro* (34), thus reinforcing the concept that PCSK9 processing is required for LDLR binding.

The LDLR EGF(AB) Domains Bind Tightly to a Region of the PCSK9 Catalytic Domain—To determine the region of PCSK9 responsible for high affinity binding to EGF(AB), we employed the "epitope excision" strategy (35). To maximize formation of the EGF(AB)-PCSK9 complex, the $PCSK9^{D374Y}$ mutant was used in these experiments. The epitope excision analysis involved several steps. First, EGF(AB) was covalently immobilized on CNBr-activated Sepharose beads and incubated with full-length PCSK9. Then, the complex was subjected to endo-

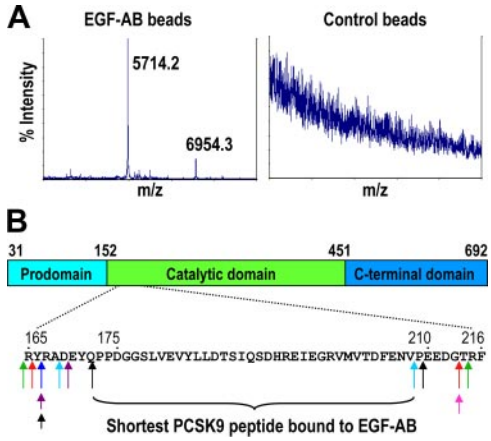

FIGURE 2. **Epitope excision and mass spectrometry analyses.** *A*, the MALDI-TOF mass spectrum of EGF(AB) beads (*left*) and control beads (*right*) after the first cycle of epitope excision employing chymotrypsin digestion. Peaks at *m/z* 5714.2 and 6954.3 result from ions corresponding to PCSK9 residues Arg-167—Phe-216 and Asn-157—Phe-216, respectively. *B*, schematic diagram of the PCSK9 domain organization and a summary of the data obtained by MS analyses. The minimal PCSK9 peptide sequence bound to EGF(AB)-coupled beads after multiple endoprotease incubations is shown. The *arrows* indicate protease cleavage sites and are color-coded. *Green*, chymotrypsin (*F*, *W*, *L*, *Y*); *red*, trypsin (*R*, *K*); *blue*, trypsin + aminopeptidase; *azure*, chymotrypsin + trypsin + GluC (*E*); *purple*, chymotrypsin + trypsin + GluC + aminopeptidase; *black*, chymotrypsin + AspN (*D*); *pink*, chymotrypsin + trypsin (*bracketed letters* indicate cleavage site specificities).

protease digestion under controlled conditions followed by a washing step. The regions of PCSK9 that bound to EGF(AB), that were protected from digestion, and that resisted washing were identified by direct analysis of the beads by MALDI MS. After one cycle of epitope excision using chymotrypsin, two predominant peptides were found associated with EGF(AB); they were identified as PCSK9 residues Asn-157—Phe-216 and Arg-167—Phe-216 (Fig. 2*A*). The latter steps of the epitope excision strategy were then repeated using additional endo- and exoproteases, enabling refinement of the results. Thus, after further cycles of digestion with trypsin, GluC, aminopeptidase, and AspN, the minimal region protected by EGF(AB) spanned PCSK9 residues Asp-175 to Glu-210 (Fig. 2*B*).

Neutral pH X-ray Structures of Wild Type PCSK9ΔC-EGF(AB) Complexes and Site-directed Mutagenesis—To characterize the molecular details of the interaction occurring between PCSK9 and LDLR we crystallized the PCSK9ΔC-EGF(AB) complex at neutral pH. The structure was determined by the molecular replacement method and was refined to 2.4 Å resolution (Table 2). No interpretable electron density was observed for the EGF(B) domain, suggesting that it is disordered in the crystals. Overall the PCSK9 and EGF(A) structures

TABLE 2

Data collection and refinement statistics

Values in parentheses correspond to the statistics for the highest resolution shell.

	PCSK9ΔC + EGF(AB)	PCSK9ΔC + EGF(AB)^{H306Y}	PCSK9ΔC^{D374Y} + EGF(AB)	PCSK9ΔC^{D374H} + EGF(AB)	PCSK9ΔC^{D374A} + EGF(AB)
Space group	$P4_32_12$	$P4_32_12$	$P4_32_12$	$P4_32_12$	$P4_32_12$
a, *b*, *c* (Å)	83.0, 83.0, 211.6	83.9, 83.9, 209.9	85.9, 85.9, 218.3	88.4, 88.4, 218.4	84.1, 84.1, 209.7
Resolution range (Å)	45–2.40 (2.53–2.40)	45–2.30 (2.42–2.30)	40–2.62 (2.76–2.62)	40–2.33 (2.46–2.33)	40–2.62 (2.76–2.62)
Reflections: total	19,1176 (25041)	233,390 (34295)	120,342 (17831)	156,846 (23254)	112647 (15328)
Reflections: unique	29,902 (4257)	33,566 (4874)	25,321 (3633)	37,593 (5426)	23184 (3341)
Completeness (%)	99.9 (99.9)	98.1 (99.7)	99.5 (99.9)	99.4 (99.8)	98.9 (99.7)
Redundancy	6.4 (5.9)	7.0 (7.0)	4.8 (4.9)	4.2 (4.3)	4.9 (4.6)
⟨Mean (*I*)/S.D.⟩	10.5 (2.1)	11.7 (2.9)	14.2 (2.3)	10.1 (2.3)	10.4 (1.8)
R_{sym} (%)	13.4 (67.9)	14.9 (63.5)	8.0 (69.5)	10.4 (59.5)	10.4 (66.8)
R_{cryst} (%)	21.5	21.8	23.3	21.9	22.6
R_{free} (%)	25.4	25.6	27.1	25.3	27.0
r.m.s.d. bond length (Å)	0.007	0.008	0.008	0.008	0.007
r.m.s.d. bond angle (°)	1.23	1.12	1.22	1.16	1.15
Surface area buried on PCSK9-EGF(A) (Å^2)	468/514	496/523	553/586	513/532	470/507
Protein Data Bank entry code	2W2M	2W2N	2W2O	2W2Q	2W2P

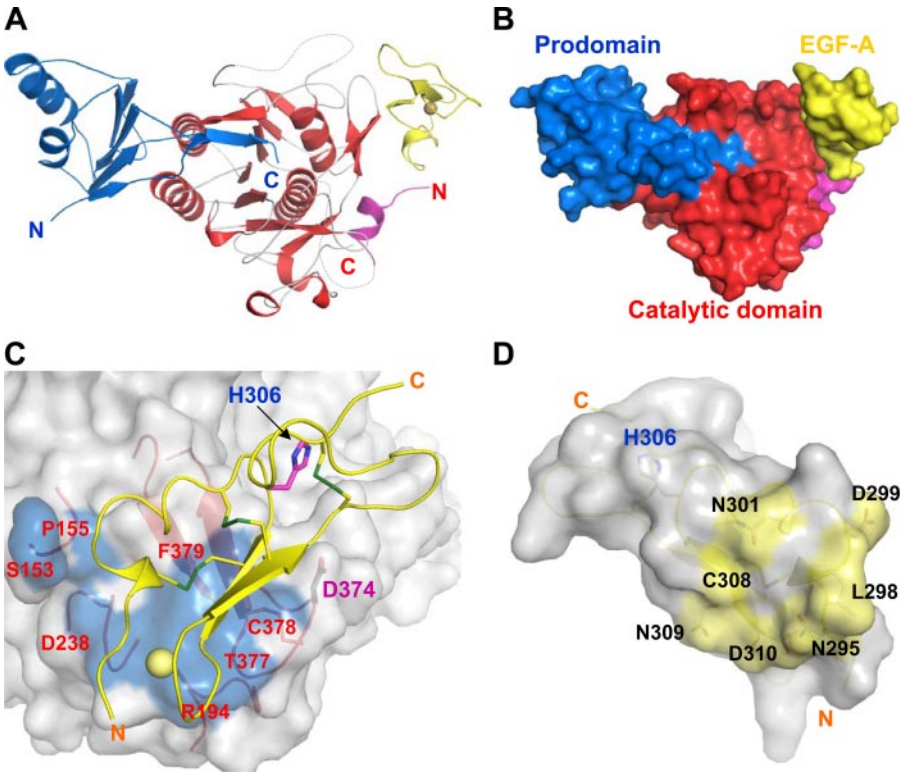

FIGURE 3. **Crystal structure of the PCSK9ΔC-EGF(AB) complex.** Ribbon (*A*) and surface (*B*) representations, in the same orientation, of the complex formed between PCSK9ΔC and EGF(A) (*yellow*). EGF(A) contacts PCSK9 via the catalytic domain (*red*) but not the prodomain (*blue*). The P′ helix, which is part of the catalytic domain, is shown in *pink*. *Dotted lines* represent PCSK9 residues for which no electron density was observed. *C*, transparent surface representation of PCSK9ΔC; *blue*-labeled patches indicate residues contacted by EGF(A) (*yellow ribbon*; the *yellow sphere* is the Ca^{2+} ion). Contacts are all less than 4 Å. Asp-374 (PCSK9) is at the tip of a β-hairpin loop. EGF(A) His-306 adopts a conformation that does not allow interaction with Asp-374 at neutral pH. Ser-153 is the N terminus of the PCSK9 catalytic domain generated upon autocleavage. Hydrogen bonds are established between side chain atoms of the following pairs of residues from PCSK9 and *EGF(A)*: Arg-194 to *Asp-310* and *Asn-295*, Asp-238 to *Asn-295*, Thr-377 to *Asn-309* and *Asp-310*, and between backbone atoms for Thr-377 to *Asp-310* and Phe-379 to *Cys-308*. *D*, transparent surface representation of EGF(A); *yellow*-labeled patches indicate residues contacted by PCSK9ΔC. The protein is oriented as if removing PCSK9ΔC from the complex shown in *panel C* followed by a 180° *y* axis rotation.

are very similar to their respective apo-structures and to the recently determined structure of the PCSK9-EGF(A) complex crystallized at pH 4.8 (r.m.s.d. values for Cα atoms are 0.4 Å for the prodomain, 0.6 Å for the catalytic domain, and 0.7 Å for EGF(A)) (20).

The EGF(A) domain makes contacts only with the catalytic domain of PCSK9, on which it buries 468 Å^2 of solvent-accessible area (Fig. 3). The interaction involves the formation of an antiparallel β-sheet between EGF(A) and the exposed side of a β-hairpin loop of PCSK9 (Fig. 3*C*). Notably, the tip of this loop is the site of the D374Y GOF mutation, which confers enhanced affinity to the interaction with LDLR. Of note, the N-terminal amino group of Ser-153 interacts with EGF(A) (Fig. 4). Importantly, the latter interaction can occur only with the processed form of the enzyme; this is consistent with the lack of LDLR binding to unprocessed PCSK9ΔC reported above.

Site-directed mutagenesis was then used to evaluate the contribution to high affinity binding of amino acids at the complex interface. When compared with the WT PCSK9ΔC protein, the PCSK9ΔC mutants R194A and D238A showed a greatly reduced ability to disrupt the PCSK9-LDLR complex (Table 3), confirming the key role of these two residues for EGF(A) binding. In addition, to assess the contribution toward EGF(A) binding of the PCSK9 P′ α-helix (generated at the N terminus of the catalytic domain following autocleavage), we expressed the PCSK9ΔC P′ mutants P155G, W156L, N157K, L158A, and I161A. These mutations are predicted to interfere with the positioning of the P′ α-helix (Fig. 4). The PCSK9ΔC P′ mutant proteins showed a strongly reduced ability to disrupt the PCSK9-LDLR interaction (Table 3), confirming the importance of the P′ α-helix for LDLR binding. Interestingly, N157K is a naturally occurring LOF mutation associated with low plasma levels of LDL cholesterol (4). Thus,

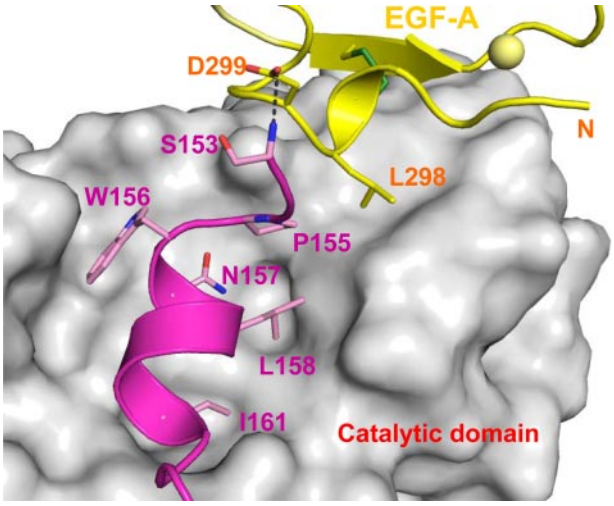

FIGURE 4. **Structural and functional role of the PCSK9 catalytic domain P′ helix.** A surface representation of the PCSK9ΔC catalytic domain (*gray*) with a ribbon representation for the P′ helix (*pink*), which is accommodated in a deep pocket of the catalytic domain after autocleavage. Ser-153 at the N terminus of the PCSK9 P′ helix makes a 2.9-Å salt bridge (shown as a *dotted line*) with the side chain of Asp-299 (EGF(A) (*yellow*)). Pro-155 makes van der Waals contacts with Leu-298 (EGF(A)). The EGF(A) Ca^{2+} ion is shown as a *sphere* and intramolecular disulfide bonds as *sticks* with sulfur in *green*). Single point mutations of residues shown on the P′ helix result in PCSK9ΔC proteins with reduced ability to disrupt the PCSK9-LDLR interaction in the TR-FRET assay (Table 3).

TABLE 3
Summary of binding data from TR-FRET assay

Protein	IC_{50}
	nM
PCSK9	80 ± 23
PCSK9ΔC	110 ± 45
PCSK9ΔC^{P155G}	1241 ± 518
PCSK9ΔC^{W156L}	1695 ± 271
PCSK9ΔC^{N157K}	850 ± 190
PCSK9ΔC^{L158A}	>2500
PCSK9ΔC^{I161A}	293 ± 2
PCSK9ΔC^{R194A}	>2500
PCSK9ΔC^{D238A}	>2500
PCSK9ΔC^{S386A}[a]	No inhibition
LDLR ectodomain	214 + 41
LDLR EGF(A)	1255 + 7
LDLR EGF(AB)	367 + 94
LDLR EGF(AB)^{H306Y}	140 ± 50

[a] Unprocessed PCSK9ΔC due to mutation of the catalytic Ser-386 to alanine. All other PCSK9 and PCSK9ΔC proteins were fully processed (autocleaved).

our binding data suggest that the phenotype of the N157K mutation is caused by a decreased affinity for the LDLR.

Molecular Basis for FH Associated with the LDLR H306Y Mutation and pH Dependence of the PCSK9-EGF(AB) Interaction—A comparison of the PCSK9ΔC-EGF(AB) neutral pH structure determined herein with the structure of the PCSK9-EGF(AB) complex determined at low pH (20) shows that although the structures are highly similar overall, EGF(A) His-306 borders the binding interface but assumes a different rotamer in the two structures. At low pH, His-306 forms an intermolecular salt bridge with the PCSK9 Asp-374 side chain, whereas at neutral pH, His-306 forms an intramolecular H-bond with the EGF(A) Ser-305 hydroxyl group (Fig. 5*A*). The His-306—Asp-374 interaction may occur at low pH following protonation of the His side chain upon traversing its pK' of ~6. Ensembles of NMR solution structures of EGF(AB) alone determined at either pH 5.5 (36) or pH 6.5 (37) all reveal a conformation of His-306 similar to that observed here at neutral pH, thus suggesting that the repositioning of His-306 requires both low pH and stabilization by the concomitant formation of a salt bridge with Asp-374. Importantly, the pH-dependent formation of this additional bond is consistent with the increased affinity of the PCSK9-EGF(AB) interaction at low pH (Table 1).

The conformational rearrangements described above also suggested that the naturally occurring LDLR mutation H306Y, which is associated with familial hypercholesterolemia (23, 24), may cause the FH phenotype by promoting enhanced PCSK9 binding. The crystal structure of PCSK9ΔC bound to EGF(AB)^{H306Y}, which we also present here (Table 2), reveals that the hydroxyl group of Tyr-306 forms an H-bond (2.8 Å) with the side chain of PCSK9 Asp-374 (Fig. 5*B*) and results in an increased total buried surface area (1019 Å^2) compared with the WT complex (982 Å^2; Table 2). The Tyr-306—Asp-374 H-bond interaction is similar to the His-306—Asp-374 salt bridge interaction observed in the low pH PCSK9-EGF(A) structure. Moreover, when tested in the TR-FRET assay, the EGF(AB)^{H306Y} mutant showed an ~3-fold enhanced binding affinity compared with WT EGF(AB) (Table 3). Of note, the Tyr-306 side chain hydroxyl group is expected to be available for H-bonding with Asp-374 regardless of the pH. Indeed, SPR studies showed that binding of PCSK9 to immobilized EGF(AB)^{H306Y} is insensitive to pH (data not shown).

We also introduced the H306Y mutation into the LDLR ectodomain protein to assess whether it abolishes the pH dependence of binding in the context of the full-length protein. In SPR experiments, the full-length LDLR^{H306Y} bound PCSK9 with a K_D of 330 nM at neutral pH, with the affinity being enhanced 50-fold (K_D = 7 nM) at acidic pH (Table 1). Therefore although pH-dependent protonation of His-306 is responsible for a modest 2–3-fold enhancement of binding affinity with PCSK9, it does not explain the large pH dependence observed for binding of PCSK9 to the full-length LDLR protein.

X-ray Crystal Structures of GOF PCSK9ΔC-EGF(AB) Complexes—Following characterization of the complex between EGF(AB) and PCSK9ΔC, we also determined the structures at neutral pH of WT EGF(AB) bound to mutant PCSK9ΔC proteins harboring the naturally occurring GOF mutations D374Y or D374H (Table 2), both of which have been reported to cause severe hypercholesterolemia (21, 22). Overall these structures are the same as the WT complex, with a Cα atom r.m.s.d. of only 0.4 Å. However, both structures reveal that at neutral pH the Tyr-374 or His-374 side chain of PCSK9ΔC establishes an H-bond (~3.2Å) with the backbone carbonyl atom of EGF(A) Cys-319 (Fig. 5, *C* and *D*). There is also a considerable increase (6–16%) in total buried surface area at the interface due to packing of the aromatic side chain of PCSK9 residue His-374/Tyr-374 against EGF(A) Leu-318 (Table 2). These additional interactions with EGF(A) may explain the enhanced affinity of the PCSK9$^{D374Y(H)}$-LDLR interactions reported previously (10, 17) and indeed the severe hypercholesterolemia in carriers of such mutations. Previously we reported a mild GOF effect for PCSK9^{D374A} (27). Not surprisingly the EGF(AB)-PCSK9^{D374A} structure (Table 2) does not reveal additional interactions of Ala-374 with EGF(AB). However, the replacement of the negatively charged Asp-374 with the non-

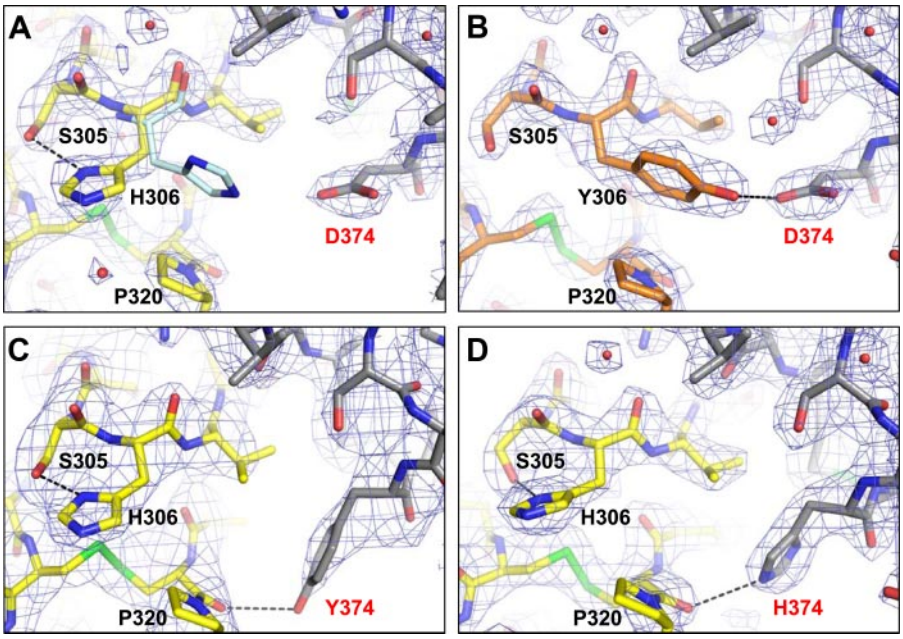

FIGURE 5. **Involvement at the binding interface of LDLR residue 306 and PCSK9 residue 374.** *A*, electron density map ($2F_o - F_c$) refined to 2.4 Å resolution (contoured at 1.5 σ), showing WT EGF(A) (*yellow*) and PCSK9ΔC (*gray*) from the structure presented here at neutral pH. The His-306 side chain Nδ atom forms a 2.8 Å hydrogen bond with the Ser-305 side chain; the Nε atom is >9 Å away from Asp-374 of PCSK9. In contrast is the conformation of the His-306 residue (*thin sticks*, *white*) from the superimposed PCSK9-EGF(A) structure determined at pH 4.8 (20). In the latter, the Nε group is ~3.9 Å from the side chain of Asp-374, presumably enabling formation of a salt bridge in the protonated state at low pH. There is no electron density visible for this low pH rotamer conformation in the map determined herein. *B*, electron density map refined to 2.3 Å resolution (1.5 σ contour), showing EGF(AB)^{H306Y} (*orange*) and PCSK9ΔC (*gray*) from the structure presented here at neutral pH. The Tyr-306 side chain does not form an H-bond to Ser-305 but rather forms a 2.8Å hydrogen bond with Asp-374 of PCSK9. The conformation of Tyr-306 at neutral pH is thus comparable with that of His-306 at low pH. *C*, electron density map refined to 2.62 Å (1 σ contour) for EGF(AB) bound to the PCSK9ΔC D374Y mutant, showing the H-bond between Tyr-374 and Cys-319. As shown in *A*, His-306 of EGF(AB) forms an intramolecular bond with Ser-305. *D*, electron density map refined to 2.33 Å (1.5 σ contour) for EGF(AB) bound to the PCSK9ΔC D374H mutant, showing the H-bond between His-374 and Cys-319.

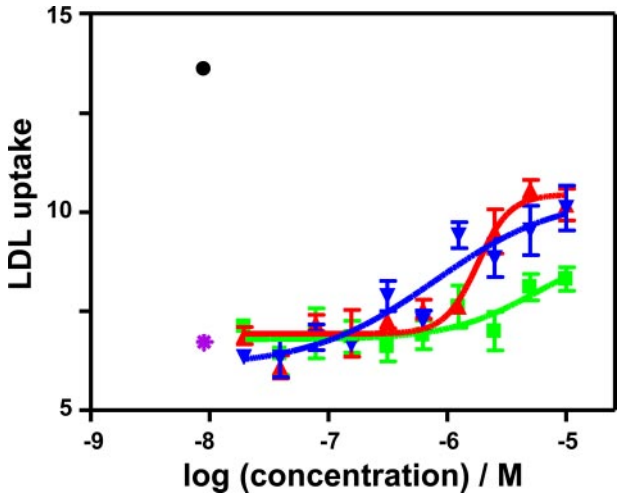

FIGURE 6. **Functional characterization of EGF(A), EGF(AB), and EGF(AB)^{H306Y} in a cell-based LDL uptake assay.** WT PCSK9 (*pink cross*) strongly reduces the amount of LDL uptake compared with background (*black-filled circle*). EGF(A) (*green square*), EGF(AB) (*red triangle*), and EGF(AB)^{H306Y} (*blue triangle*) inhibit the effect of WT PCSK9. The effect of soluble LDLR ectodomain could not be measured in this assay because of its intrinsic ability to bind LDL.

polar Ala-374 may favor formation of the interface, given the hydrophobic nature of the environment around EGF(AB) residues Val-307 and Leu-318 (supplemental Fig. 2).

Functional Characterization of EGF(A) and EGF(AB) WT and H306Y Mutant—Previous work has established that the addition of purified mature PCSK9 to the medium of cultured cells causes a lowering of LDL uptake due to a down-regulation of LDLR protein levels (9, 14, 17). To determine whether the EGF(A) and EGF(AB) repeats could inhibit the LDLR-lowering activity of exogenously added PCSK9, we tested the effect of these two proteins in a cellular LDL uptake assay. Here we demonstrated that isolated EGF(A) and EGF(AB) proteins are sufficient to inhibit the LDLR-lowering effect of purified PCSK9 added exogenously to cultured cells, with IC_{50} values of 5.4 ± 1.5 and 1.5 ± 0.5 μM, respectively. Moreover, the mutant EGF(AB)^{H306Y} protein was an even more potent inhibitor of PCSK9 (IC_{50} = 0.8 μM) (Fig. 6). These values reflect the relative potencies reported above for inhibition of the PCSK9-LDLR interaction by EGF(A), EGF(AB), and EGF(AB)^{H306Y} in the TR-FRET assay.

DISCUSSION

The identification of mutations in *PCSK9* that are associated with either hypercholesterolemia or hypocholesterolemia has generated a great interest in the biology of PCSK9 and its mechanism of action. As for other convertases, PCSK9 undergoes an autocleavage event that is required for its secretion (8, 9). Following autocleavage, the protease activity of mature PCSK9 appears to be self-inhibited by the prodomain, which remains stably associated with the rest of the protein (10–12). Mature PCSK9 acts by binding to LDLR at the cell surface and subsequently promoting internalization and degradation of the receptor, an activity that is independent of its catalytic triad (34, 38). The binding of PCSK9 to LDLR is therefore fundamental in reducing receptor levels. Here we report a biochemical, structural, and functional characterization of this interaction, thus providing insight into molecular determinants governing the regulation of circulating LDL levels.

It has been shown previously that the EGF(A) repeat of LDLR is sufficient for PCSK9 binding (19, 20). Moreover, our binding studies indicate that the PCSK9 C-terminal domain is not involved in the interaction with LDLR, as a PCSK9ΔC protein lacking this region of the protein showed approximately the same affinity for the receptor as full-length PCSK9. Thus, to characterize the molecular details of the interaction between PCSK9 and LDLR, we crystallized the PCSK9ΔC-EGF(AB) complex at neutral pH. In the structure the EGF(A) domain was

found to contact only the catalytic domain of PCSK9 in proximity to a β-hairpin loop containing residue Asp-374. A naturally occurring D374Y GOF mutation conferred a higher affinity of binding to the LDLR. The observed mode of binding was consistent with our biochemical and functional data. Indeed, despite its small size, the EGF(A) repeat (40 amino acids) competed efficiently with full-length LDLR ectodomain (766 amino acids) for binding to PCSK9. We note that in our TR-FRET assay, EGF(AB) (80 residues) was slightly more potent than EGF(A); it is likely that this difference was due to the greater structural stability of the EGF(AB) protein rather than to a significant increase in the number of residues directly involved in binding.

A panel of mutant PCSK9ΔC proteins was produced to assess the contribution of single amino acids at the complex interface for high affinity binding. This approach further validated the structural findings and confirmed the key role of PCSK9 Arg-194, which binds to EGF(A) Asp-310, and PCSK9 Asp-238, which forms a hydrogen bond with EGF(A) Asn-295. In addition the structure and mutagenesis data suggested an essential role in LDLR binding for the P′ α-helix at the N terminus of the PCSK9 catalytic domain. Indeed, PCSK9ΔC proteins containing mutations predicted to affect the position and/or structure of this α-helix were found to undergo normal autoprocessing but were defective in LDLR binding. Among these mutants is the naturally occurring N157K variant, thus providing an explanation for the associated LOF phenotype.

The interaction of PCSK9 with EGF(A) has been shown to be pH-dependent (19, 20). Our SPR studies confirmed that the EGF(AB) domain has an increased binding affinity for PCSK9 at low pH, although this increase was smaller than that observed for the full-length LDLR ectodomain (*i.e.* 3-fold *versus* ~100-fold). The increased affinity of the interaction at acidic pH is of mechanistic relevance, and therefore residues responsible for this behavior are of particular interest. Although most of the intermolecular contacts are mediated by polar residues that are unlikely to change their protonation state when moving from physiological pH to acidic pH, a histidine of EGF(A), His-306, is located at the border of the EGF(A) region binding PCSK9. Because histidine side chains typically have a p*K*′ value of ~6, the amino acid His-306 has been suggested to mediate the pH dependence of PCSK9-EGF(AB) binding (20). At the neutral pH of our structure, the side chain of His-306 is presumably unprotonated, and the Nδ atom accepts an intramolecular H-bond (2.8Å) from the side chain OH group of Ser-305 (Fig. 5*A*). This arrangement differs from the conformation adopted by the His-306 side chain in the crystal structure of the complex between WT PCSK9 and EGF(AB) determined at pH 4.8 (20). In the low pH structure, His-306 does not form an H-bond with Ser-305 but rather points toward PCSK9 Asp-374. At pH 4.8, it is highly likely that His-306 becomes protonated and positively charged, thereby allowing formation of a salt bridge (3.5–4.0Å) with the carboxylate group of Asp-374. Formation of this interaction also results in an increase in total buried surface. The stabilization of this alternative rotamer conformation of His-306 appears to be dependent on the presence of PCSK9, because in NMR structures determined previously at pH 5.5 the His-306 side chain is in a position similar to the one observed here at neutral pH. The pH-dependent formation of the additional salt bridge and increase in buried surface area represents a potential mechanism for affinity enhancement of the PCSK9-EGF(A) interaction during endocytosis and transfer of the complex from neutral pH to the acidic pH of the endosomes.

The model described above suggests that the pH-dependent enhancement of the PCSK9-EGF(A) interaction is linked to the formation of a salt bridge between Asp-374 and His-306 and to an increase in the total buried surface of the complex. This hypothesis is supported by the structures of PCSK9ΔC-EGF(AB)^{H306Y}, PCSK9ΔC^{D374Y}-EGF(AB), and PCSK9ΔC^{D374H}-EGF(AB) complexes obtained at neutral pH. In the PCSK9ΔC-EGF(AB)^{H306Y} structure, the Tyr-306 side chain adopts a rotamer conformation similar to the one observed for His-306 in the low pH PCSK9-EGF(AB) complex and with its hydroxyl group establishes a hydrogen bond with the Asp-374 side chain (Fig. 5*B*). When tested in the TR-FRET assay, this EGF(AB) mutant showed a 3-fold enhancement in affinity for PCSK9, further confirming that formation of a bond with PCSK9 Asp-374 results in a tighter association of the complex. Importantly, the increased PCSK9 binding activity of EGF(AB)^{H306Y} is in close agreement with the ~3-fold enhancement at pH 5.6–6.0 of the PCSK9-EGF(AB) affinity (Ref. 20 and this study). Similar to the PCSK9ΔC-EGF(AB)^{H306Y} complex, in the PCSK9ΔC^{D374Y}-EGF(AB) complex an additional hydrogen bond is formed between the Tyr-374 hydroxyl group and the carbonyl oxygen of EGF(A) Cys-319. Further, there is a significant (16%) increase in the total buried surface area due to the involvement of the large Tyr-374 side chain. Together these observations may explain the 6–30-fold tighter LDLR binding of this PCSK9 GOF mutant compared with the WT protein at neutral pH (10, 17). A similar interaction is established by the His-374 side chain in the PCSK9ΔC^{D374H}-EGF(AB) complex, presumably explaining the GOF phenotype associated with this FH mutant PCSK9.

The interaction between PCSK9^{D374Y} and EGF(AB) is also pH-dependent (supplemental Fig. 1*B*) (10, 17). As proposed previously (20), at acidic pH the protonated EGF(A) His-306 side chain may adopt the conformation observed in the low pH PCSK9-EGF(AB) structure, thus establishing an intermolecular hydrogen bond to PCSK9 Tyr-374. The interaction between Tyr-374 and His-306 could be shorter (~2.9Å) than that established at neutral pH with Cys-319 (~3.2Å) and would also cause a further increase in the total buried surface, potentially explaining the enhancement in binding affinity at acidic pH for this complex. Thus, formation of an H-bond at neutral pH between Asp-374 and EGF(A) Tyr-306, or between Tyr-374 or His-374 and the carbonyl oxygen of EGF(A) Cys-319, and formation of a salt bridge at low pH between Asp-374 and EGF(A) His-306 have similar effects in increasing the affinity of the complex. Nevertheless, we note that mutation of Asp-374 into Ala or Phe has also been reported to result in an increased affinity for the LDLR (27) suggesting that other factors, such as electrostatic effects, might also modulate the affinity of the complex.

Together these data support the notion that the protonation of EGF(A) His-306 and formation of an intermolecular salt

bridge with Asp-374 are responsible for the pH dependence of the PCSK9-EGF(A) interaction. Consistently, in SPR experiments we found that the affinity of the PCSK9-EGF(AB)^{H306Y} interaction is pH-independent (data not shown; see "Results"). Importantly a 50-fold increase in PCSK9 binding at low pH compared with neutral pH was observed when studying the same H306Y mutation in the full-length LDLR ectodomain, demonstrating that additional factors contribute to the large increase in affinity of the PCSK9-LDLR complex observed at low pH. Changes in the conformation of the LDLR and increased accessibility of the EGF(A) domain to PCSK9, as indicated by a faster association constant (k_{on}) at low pH compared with neutral pH (Table 1 and Ref. 17), may in part explain the large increase in binding affinity observed at acidic pH. Moreover, the much greater affinity at acidic pH seen for the PCSK9-LDLR complex compared with PCSK9-EGF(AB) complex points to additional factors, such as an increased number of contacts or greater structural rigidity of the EGF(A) domain within the full-length LDLR, which may play a role in the interaction.

In an extension of our biochemical analyses to a cellular context, we also demonstrated that EGF(A) and EGF(AB) are sufficient to inhibit the LDLR-lowering activity of PCSK9 in a cell-based assay that monitors the uptake of LDL. In the same functional assay the EGF(AB)^{H306Y} mutant was even more potent than EGF(AB), supporting our structural and biochemical results. Importantly, this is the first demonstration that the activity of exogenous PCSK9 can be inhibited by direct competition of its interaction with LDLR. Of note, epitope excision and mass spectrometry using PCSK9 and the PCSK9-EGF(AB) complex revealed that PCSK9 residues 175–210 remain bound to EGF(AB) after protease treatment and washing, suggesting that they bind tightly to EGF(AB). It will be interesting to test whether peptides based on this single region of the PCSK9 catalytic domain may bind the EGF(A) domain with sufficiently high affinity to interfere with the PCSK9-LDLR interaction. Likewise, peptidic fragments of EGF(A) might bind PCSK9 and have inhibitory potential.

In summary, the results presented herein provide the molecular basis for the interaction of PCSK9 with the LDLR EGF(A) domain occurring at the cell surface at neutral pH. The structures of several complexes containing mutations associated with FH reveal the mechanism for enhanced PCSK9-LDLR interactions leading to gain-of-function phenotypes and hypercholesterolemia. Further, the structural and biochemical data lead to a plausible model for the determinants of the pH dependence of this interaction. Finally, we have demonstrated that the EGF subfragments of the LDLR are able to counteract the inhibitory effect of PCSK9 in LDL uptake assays, but further efforts are required to employ the structural and biochemical data presented herein for the development of disruptors of the PCSK9-LDLR interaction that appear to hold therapeutic promise.

REFERENCES

1. Abifadel, M., Varret, M., Rabes, J. P., Allard, D., Ouguerram, K., Devillers, M., Cruaud, C., Benjannet, S., Wickham, L., Erlich, D., Derre, A., Villeger, L., Farnier, M., Beucler, I., Bruckert, E., Chambaz, J., Chanu, B., Lecerf, J. M., Luc, G., Moulin, P., Weissenbach, J., Prat, A., Krempf, M., Junien, C., Seidah, N. G., and Boileau, C. (2003) *Nat. Genet.* **34,** 154–156
2. Leren, T. P. (2004) *Clin. Genet.* **65,** 419–422
3. Cohen, J., Pertsemlidis, A., Kotowski, I. K., Graham, R., Garcia, C. K., and Hobbs, H. H. (2005) *Nat. Genet.* **37,** 161–165
4. Berge, K. E., Ose, L., and Leren, T. P. (2006) *Arterioscler. Thromb. Vasc. Biol.* **26,** 1094–1100
5. Cameron, J., Holla, O. L., Laerdahl, J. K., Kulseth, M. A., Ranheim, T., Rognes, T., Berge, K. E., and Leren, T. P. (2008) *J. Intern. Med.* **263,** 420–431
6. Kotowski, I. K., Pertsemlidis, A., Luke, A., Cooper, R. S., Vega, G. L., Cohen, J. C., and Hobbs, H. H. (2006) *Am. J. Hum. Genet.* **78,** 410–422
7. Cohen, J. C., Boerwinkle, E., Mosley, T. H., Jr., and Hobbs, H. H. (2006) *N. Engl. J. Med.* **354,** 1264–1272
8. Seidah, N. G., Benjannet, S., Wickham, L., Marcinkiewicz, J., Jasmin, S. B., Stifani, S., Basak, A., Prat, A., and Chretien, M. (2003) *Proc. Natl. Acad. Sci. U. S. A.* **100,** 928–933
9. Cameron, J., Holla, O. L., Ranheim, T., Kulseth, M. A., Berge, K. E., and Leren, T. P. (2006) *Hum. Mol. Genet.* **15,** 1551–1558
10. Cunningham, D., Danley, D. E., Geoghegan, K. F., Griffor, M. C., Hawkins, J. L., Subashi, T. A., Varghese, A. H., Ammirati, M. J., Culp, J. S., Hoth, L. R., Mansour, M. N., McGrath, K. M., Seddon, A. P., Shenolikar, S., Stutzman-Engwall, K. J., Warren, L. C., Xia, D., and Qiu, X. (2007) *Nat. Struct. Mol. Biol.* **14,** 413–419
11. Hampton, E. N., Knuth, M. W., Li, J., Harris, J. L., Lesley, S. A., and Spraggon, G. (2007) *Proc. Natl. Acad. Sci. U. S. A.* **104,** 14604–14609
12. Piper, D. E., Jackson, S., Liu, Q., Romanow, W. G., Shetterly, S., Thibault, S. T., Shan, B., and Walker, N. P. (2007) *Structure* (*Lond.*) **15,** 545–552
13. Horton, J. D., Cohen, J. C., and Hobbs, H. H. (2007) *Trends Biochem. Sci.* **32,** 71–77
14. Lagace, T. A., Curtis, D. E., Garuti, R., McNutt, M. C., Park, S. W., Prather, H. B., Anderson, N. N., Ho, Y. K., Hammer, R. E., and Horton, J. D. (2006) *J. Clin. Investig.* **116,** 2995–3005
15. Grefhorst, A., McNutt, M. C., Lagace, T. A., and Horton, J. D. (2008) *J. Lipid Res.* **49,** 1303–1311
16. Schmidt, R. J., Beyer, T. P., Bensch, W. R., Qian, Y. W., Lin, A., Kowala, M., Alborn, W. E., Konrad, R. J., and Cao, G. (2008) *Biochem. Biophys. Res. Commun.* **370,** 634–640
17. Fisher, T. S., Lo Surdo, P., Pandit, S., Mattu, M., Santoro, J. C., Wisniewski, D., Cummings, R. T., Calzetta, A., Cubbon, R. M., Fischer, P. A., Tarachandani, A., De Francesco, R., Wright, S. D., Sparrow, C. P., Carfi, A., and Sitlani, A. (2007) *J. Biol. Chem.* **282,** 20502–20512
18. Nassoury, N., Blasiole, D. A., Tebon Oler, A., Benjannet, S., Hamelin, J., Poupon, V., McPherson, P. S., Attie, A. D., Prat, A., and Seidah, N. G. (2007) *Traffic* **8,** 718–732
19. Zhang, D. W., Lagace, T. A., Garuti, R., Zhao, Z., McDonald, M., Horton, J. D., Cohen, J. C., and Hobbs, H. H. (2007) *J. Biol. Chem.* **282,** 18602–18612
20. Kwon, H. J., Lagace, T. A., McNutt, M. C., Horton, J. D., and Deisenhofer, J. (2008) *Proc. Natl. Acad. Sci. U. S. A.* **105,** 1820–1825
21. Naoumova, R. P., Tosi, I., Patel, D., Neuwirth, C., Horswell, S. D., Marais, A. D., van Heyningen, C., and Soutar, A. K. (2005) *Arterioscler. Thromb. Vasc. Biol.* **25,** 2654–2660
22. Bourbon, M., Alves, A. C., Medeiros, A. M., Silva, S., and Soutar, A. K. (2008) *Atherosclerosis* **196,** 633–642
23. Day, I. N., Whittall, R. A., O'Dell, S. D., Haddad, L., Bolla, M. K., Gudnason, V., and Humphries, S. E. (1997) *Hum. Mutat.* **10,** 116–127
24. Fouchier, S. W., Defesche, J. C., Umans-Eckenhausen, M. W., and Kastelein, J. P. (2001) *Hum. Genet.* **109,** 602–615
25. Malby, S., Pickering, R., Saha, S., Smallridge, R., Linse, S., and Downing, A. K. (2001) *Biochemistry* **40,** 2555–2563
26. van den Berg, S., Lofdahl, P. A., Hard, T., and Berglund, H. (2006) *J. Biotechnol.* **121,** 291–298
27. Pandit, S., Wisniewski, D., Santoro, J. C., Ha, S., Ramakrishnan, V., Cubbon, R. M., Cummings, R. T., Wright, S. D., Sparrow, C. P., Sitlani, A., and Fisher, T. S. (2008) *J. Lipid Res.* **49,** 1333–1343
28. Leslie, A. G. W. (1992) *Joint CCP4 + ESF-EAMCB Newsletter on Protein Crystallography* **26**
29. CCP4. (1994) *Acta Crystallogr. Sect. D Biol. Crystallogr.* **50,** 760–763

30. McCoy, A. J., Grosse-Kunstleve, R. W., Storoni, L. C., and Read, R. J. (2005) *Acta Crystallogr. Sect. D Biol. Crystallogr.* **61,** 458–464
31. Emsley, P., and Cowtan, K. (2004) *Acta Crystallogr. Sect. D Biol. Crystallogr.* **60,** 2126–2132
32. Murshudov, G. N., Vagin, A. A., and Dodson, E. J. (1997) *Acta Crystallogr. Sect. D Biol. Crystallogr.* **53,** 240–255
33. Krissinel, E., and Henrick, K. (2007) *J. Mol. Biol.* **372,** 774–797
34. McNutt, M. C., Lagace, T. A., and Horton, J. D. (2007) *J. Biol. Chem.* **282,** 20799–20803
35. Jeyarajah, S., Parker, C. E., Summer, M. T., and Tomer, K. B. (1998) *J. Am. Soc. Mass Spectrom.* **9,** 157–165
36. Kurniawan, N. D., Aliabadizadeh, K., Brereton, I. M., Kroon, P. A., and Smith, R. (2001) *J. Mol. Biol.* **311,** 341–356
37. Saha, S., Boyd, J., Werner, J. M., Knott, V., Handford, P. A., Campbell, I. D., and Downing, A. K. (2001) *Structure* (*Lond.*) **9,** 451–456
38. Li, J., Tumanut, C., Gavigan, J. A., Huang, W. J., Hampton, E. N., Tumanut, R., Suen, K. F., Trauger, J. W., Spraggon, G., Lesley, S. A., Liau, G., Yowe, D., and Harris, J. L. (2007) *Biochem. J.* **406,** 203–207

Structural and Biochemical Characterization of the Wild Type PCSK9-EGF(AB) Complex and Natural Familial Hypercholesterolemia Mutants

Matthew J. Bottomley, Agostino Cirillo, Laura Orsatti, Lionello Ruggeri, Timothy S. Fisher, Joseph C. Santoro, Richard T. Cummings, Rose M. Cubbon, Paola Lo Surdo, Alessandra Calzetta, Alessia Noto, Jennifer Baysarowich, Marco Mattu, Fabio Talamo, Raffaele De Francesco, Carl P. Sparrow, Ayesha Sitlani and Andrea Carfí

J. Biol. Chem. 2009, 284:1313-1323.
doi: 10.1074/jbc.M808363200 originally published online November 10, 2008
